Full Multimodal Analysis of an Open Rectangular Groove Waveguide

Mark Fernyhough and David V. Evans

***Abstract*—In this paper, a full multimodal analysis of an open rectangular-shaped groove waveguide is presented for both TE and TM modes. The method of solution involves the formulation of the problem in terms of an integral-equation representation to which a Galerkin approximation, which incorporates the anticipated singularities at the edges of the guide, is then applied. The method proves to be extremely accurate and numerically efficient to compute, and results are presented for both the lower and higher order modes.**

***Index Terms*—Groove guide, microwaves, multimodal.**

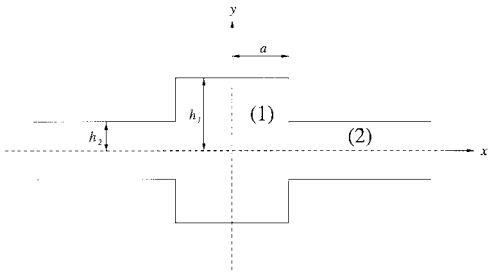

Fig. 1. Cross section of groove guide.

I. Introduction

THE GROOVE waveguide was first considered by Tischer [1] for use at millimeter wavelengths as an alternative to classical waveguides such as the H-guide and the rectangular guide. It has many advantages such as low-loss low dimensional tolerance and the ability to handle higher power capacities at high frequencies. Most of these properties are attributed to the open endedness of the guide, which reduces wall losses. The grooves in the guide trap the fields locally and prevent radiation leaking out along the open parts of the guide.

Many authors have studied the groove guide both experimentally and analytically. Conformal mapping techniques have been used by Tischer [1], Bava and Perona [2], and Choi *et al*. [3]. The mapping of the region enclosed by the groove guide into the region between two parallel planes results in a Helmholtz equation with the space-varying wavenumber corresponding to an anisotropic medium for which approximate methods need to be employed. Thus, Bava and Perona chose the shape of the groove to make analysis easier, from which approximate values of the cutoff wavelengths were obtained using a stationary expression for the cutoff wavenumber. A different approach was used for the rectangular groove guide by Nakahara and Kurauchi [4], [5] who presented both theory and experimental results. They were able to obtain first-order results by using only the dominant mode in each region of the groove to produce a dispersion equation. Although their analysis was approximate, the results obtained gave fair agreement with their carefully measured experimental results. Subsequently, Oliner and Lampariello [6] using a new transverse equivalent network formulation for the rectangular groove guide were able to provide a simple dispersion relation for the properties of the dominant mode. Even though the results are approximate (the susceptance is assumed to be constant) the dispersion relation was in an extremely simple form, and when compared to experimental data produced much more accurate results than previous methods. Mahmoud [7], [8] employed an approximate mode-matching scheme to the problem, which used the full solution in the groove region, but only a simple modal expression for the open-ended region. He was able to manipulate the resulting dispersion relation into a form analogous to that of Oliner and Lampariello in which the value of the susceptance was dependent upon the geometry of the guide and was not constant, as assumed by Oliner and Lampariello. The most accurate solutions to date are by Sachidananda [9] who analyzed the groove guide using a mode-matching technique employing three domains in place of the two domains used conventionally. The method, which is accurate to about two or three places of accuracy after truncation of the resulting infinite system of equations, only applies to the dominant TE mode. Other important work in this area is due to Ma, Yamashita, and Xu [10], and Ma and Yamashita [11], [12]. In [10], they consider arbitrary groove profiles, and in [11] and [12], leaky-wave characteristics are studied due to the insertion of a strip into the rectangular groove waveguide.

In this paper, we present the full multimodal solutions for the rectangular groove waveguide, where we allow more than one wave-like mode trapped locally around the groove region. In total, there are six types of solutions to this problem due to the symmetry of the guide (see Fig. 1), consisting of two TE solutions antisymmetric about $y = 0$ (symmetric and antisymmetric about $x = 0$) and four sets of TM solutions exploiting all combinations of the symmetries about $x = 0$ and $y = 0$.

Manuscript received April 25, 1996; revised October 9, 1997.

M. Fernyhough was with the Applied Mathematics and Numerical Analysis Group, School of Mathematics, University of Bristol, Bristol BS8 1TW, U.K. He is now with the Target Echo Strength Group, Defence Evaluation and Research Agency, Winfrith Technology Center, Dorset DT2 8XJ U.K.

D. V. Evans is with the Applied Mathematics and Numerical Analysis Group, School of Mathematics, University of Bristol, Bristol BS8 1TW, U.K.

Publisher Item Identifier S 0018-9480(98)00621-8.

In Section II, the problem is formulated in terms of an integral equation, and instead of seeking an exact solution, a Galerkin approximation is used in which expansion functions are chosen to model the behavior at the end points of the integral corresponding to the edges of the rectangular groove, and also chosen to provide maximum simplification of the results. The same method has been employed in similar problems (e.g., [13], [14]). Although the method of solution at first glance appears to be mathematically complex, the final form is simple and the problem is reduced to finding zeros of a determinant corresponding to values of the cutoff frequency. The method turns out to be extremely efficient with no more than five expansion functions needed to give results to at least six-figure accuracy. In fact, as we increase the number of expansion functions, the results converge extremely rapidly.

In Section III, results are presented showing the convergence of the ratio of free-space wavelength to guide wavelength compared with Sachidananda's [9] three domain mode-matching solution. Oliner's [6] transverse equivalent network and Nakahara and Kurauchi's [4], [5] first-order theory and experiments are also compared. Results are also presented for various TE- and TM-mode solutions including geometries of the groove guide where multiple cutoff frequencies exist, and an approximation for arbitrarily shaped groove guides (derived in the Appendix) is used for comparison when the groove width is small.

II. Formulation and Solution

Cartesian coordinates are chosen and the dimensions of the groove guide are illustrated in Fig. 1, with the z-axis measured into the page. We assume that the solutions of Maxwell's equations are time-harmonic with angular frequency ω and that the motion in the z-direction along the groove guide is periodic with wavenumber β. We seek solutions for the electric and magnetic Hertzian potentials (corresponding to TM and TE solutions, respectively). In an obvious notation, we write

$$\boldsymbol{\Phi}_{e,h} = \hat{\boldsymbol{a}}_z \phi_{e,h}(x,y) e^{-i\beta z} \tag{1}$$

where, within the interior of the waveguide, $\phi_{e,h}(x,y)$ satisfies

$$\left(\frac{\partial^2}{\partial x^2} + \frac{\partial^2}{\partial y^2} + k_c^2\right)\phi_{e,h}(x,y) = 0 \tag{2}$$

and on the walls of the waveguide

$$\phi_e = 0 \quad \frac{\partial \phi_h}{\partial n} = 0. \tag{3}$$

Also, we require that the guided waves are contained locally around the recessive groove in the waveguide and, thus, require that $\phi_{e,h}$ satisfy the radiation condition

$$\phi_{e,h} \to 0 \quad \text{as } |x| \to \infty. \tag{4}$$

Here, $\hat{\boldsymbol{a}}_z$ is the unit vector in the z-direction and $k_c^2 = k_0^2 - \beta^2$ is the cutoff wavenumber with $k_0 = \omega/c_0$ the free-space wavenumber and c_0 the speed of light. The electric- and magnetic-field vectors can be related to either the electric or magnetic Hertzian potentials (see [15]) by

$$\boldsymbol{E} = \nabla \times \nabla \times \boldsymbol{\Phi}_e \quad \boldsymbol{H} = i\omega\epsilon_0 \nabla \times \boldsymbol{\Phi}_e \tag{5}$$

for the TM solution or for the TE solution

$$\boldsymbol{E} = -i\mu_0\omega \nabla \times \boldsymbol{\Phi}_h \quad \boldsymbol{H} = \nabla \times \nabla \times \boldsymbol{\Phi}_h. \tag{6}$$

Here, μ_0 and ϵ_0 are the permeability and permittivity, respectively, of free space. Note from Fig. 1 that the geometry has two lines of symmetry, namely at $x = 0$ and $y = 0$, so we only need to consider the quadrant $x \geq 0, y \geq 0$ with the appropriate symmetry conditions at $x = 0$ and $y = 0$. For both the TE and TM modes there exists symmetric and antisymmetric solutions about $x = 0$, but for the symmetry about $y = 0$ there is only an antisymmetric set of TE modes satisfying (4) (the symmetric about $y = 0$ set of TE modes always have traveling wave solutions as $x \to \pm\infty$) while both symmetric and antisymmetric solutions exist about $y = 0$ for the TM modes. Thus, in total there exists six sets of solutions to this problem.

We now split the region into two (see Fig. 1). Region (1) is defined by $0 \leq y \leq h_1, 0 \leq x \leq a$ while region (2) is given by $0 \leq y \leq h_2, x \geq a$. The general form of solutions in regions (1) and (2) for the TE modes antisymmetric about $y = 0$ are

$$\phi_h^{(1)} = \sum_{n=1}^{\infty} \frac{U_n^{(1)}}{P_{1n}} \chi(x, P_{1n}) \psi_{1n}^{h,a}(y) \tag{7}$$

and

$$\phi_h^{(2)} = -\sum_{n=1}^{\infty} \frac{U_n^{(2)}}{P_{2n}} e^{-P_{2n}(x-a)} \psi_{2n}^{h,a}(y). \tag{8}$$

Similarly, for the antisymmetric TM modes about $y = 0$, the general solutions in regions (1) and (2) are

$$\phi_e^{(1)} = \sum_{n=1}^{\infty} \frac{U_n^{(1)}}{Q_{1n}} \chi(x, Q_{1n}) \psi_{1n}^{e,a}(y) \tag{9}$$

$$\phi_e^{(2)} = -\sum_{n=1}^{\infty} \frac{U_n^{(2)}}{Q_{2n}} e^{-Q_{2n}(x-a)} \psi_{2n}^{e,a}(y) \tag{10}$$

and for the TM modes symmetric about $y = 0$

$$\phi_e^{(1)} = \sum_{n=1}^{\infty} \frac{U_n^{(1)}}{P_{1n}} \chi(x, P_{1n}) \psi_{1n}^{e,s}(y) \tag{11}$$

$$\phi_e^{(2)} = -\sum_{n=1}^{\infty} \frac{U_n^{(2)}}{P_{2n}} e^{-P_{2n}(x-a)} \psi_{2n}^{e,s}(y). \tag{12}$$

Here, $U_m^{(1)}, U_m^{(2)}$ are as yet unknown and we have defined

$$\chi(x,t) = \left\{ \begin{matrix} \dfrac{\cosh tx}{\sinh ta} \\ \dfrac{\sinh tx}{\cosh ta} \end{matrix} \right\} \text{for} \left\{ \begin{matrix} \text{symmetric} \\ \text{anti-symmetric} \end{matrix} \right\} \tag{13}$$

solutions about $x = 0$, where we assume t is a constant, thus

$$\left.\frac{d\chi}{dx}\right|_{x=a} = t. \tag{14}$$

The eigenfunctions are defined for $i = 1, 2, n = 1, 2, \cdots$, by

$$\begin{aligned} \psi_{\mathbf{in}}^{h,a} &= \sqrt{2}\sin p_{\mathbf{in}} y \\ \psi_{\mathbf{in}}^{e,a} &= \sqrt{2}\sin q_{\mathbf{in}} y \\ \psi_{\mathbf{in}}^{e,s} &= \sqrt{2}\cos p_{\mathbf{in}} y \end{aligned} \tag{15}$$

where for $i = 1,2, n = 1,2,\cdots$

$$p_{\mathbf{in}} = \left(n - \frac{1}{2}\right)\frac{\pi}{h_i}, \quad q_{\mathbf{in}} = \frac{n\pi}{h_i} \tag{16}$$

and (15) are orthogonal in the sense that

$$\frac{1}{h_i}\int_0^{h_i} \psi_{im}(y)\psi_{\mathbf{in}}(y)\,dy = \delta_{mn}. \tag{17}$$

Finally, for $i = 1,2, n = 1,2,\cdots$

$$P_{\mathbf{in}} = (p_{\mathbf{in}}^2 - k_c^2)^{1/2} \quad Q_{\mathbf{in}} = (q_{\mathbf{in}}^2 - k_c^2)^{1/2}. \tag{18}$$

Returning to (8), (10), (12), (16), and (18) we see that in order for (4) to be satisfied we choose $k_c < \pi/2h_2$ for the antisymmetric TE mode while for the antisymmetric and symmetric TM modes $k_c < \pi/h_2$ and $k_c < \pi/2h_2$, respectively.

We will only consider the analysis for antisymmetric TE solutions, as the method is similar for the TM solutions for which changes will be outlined later.

The general solutions for regions (1) and (2) need to be matched at their common boundary $x = a$. Continuity of $\partial\phi_h/\partial x$ at $x = a, 0 \le y \le h_1$ gives

$$\left.\frac{\partial\phi_h}{\partial x}\right|_{x=a} = U(y) = \sum_{n=1}^{\infty} U_n^{(1)}\psi_{1n}^{h,a}(y) = \begin{cases} \displaystyle\sum_{n=1}^{\infty} U_n^{(2)}\psi_{2n}^{h,a}(y), & y \in [0, h_2] \\ 0, & y \in [h_2, h_1] \end{cases} \tag{19}$$

where $U(y)$ has been introduced. Using the orthogonality of $\psi_{\mathbf{in}}^{h,a}(y)$ from (17) we find

$$U_n^{(i)} = \frac{1}{h_i}\int_0^{h_2} U(y)\psi_{\mathbf{in}}^{h,a}(y)\,dy, \qquad i = 1,2 \tag{20}$$

where we have used the fact that $U(y) = 0, y \in [0, h_2]$.

Continuity of ϕ_h for $x = a, y \in [0, h_2]$ now requires

$$\sum_{n=1}^{\infty} \frac{U_n^{(1)}}{P_{1n}}\chi(a, P_{1n})\psi_{1n}^{h,a}(y) + \sum_{n=1}^{\infty} \frac{U_n^{(2)}}{P_{2n}}\psi_{2n}^{h,a}(y) = 0. \tag{21}$$

Substituting (20) into (21) we find

$$\int_0^{h_2} U(t)\left\{\sum_{n=1}^{\infty} \frac{\chi(a, P_{1n})}{P_{1n}h_1}\psi_{1n}^{h,a}(y)\psi_{1n}^{h,a}(t) + \sum_{n=1}^{\infty} \frac{1}{P_{2n}h_2}\psi_{2n}^{h,a}(y)\psi_{2n}^{h,a}(t)\right\} dt = 0. \tag{22}$$

Let us now multiply (22) by $U(y)$ and integrate over $[0, h_2]$ to obtain

$$\sum_{n=1}^{\infty} \frac{\chi(a, P_{1n})}{P_{1n}h_1}\left(\int_0^{h_2} U(y)\psi_{1n}^{h,a}(y)\,dy\right)^2 + \sum_{n=1}^{\infty} \frac{1}{P_{2n}h_2}\left(\int_0^{h_2} U(y)\psi_{2n}^{h,a}(y)\,dy\right)^2 = 0. \tag{23}$$

We see from (23) that if P_{1n} is real and positive (i.e., $k_c < p_{11}$) then the kernel of (22) is positive definite and, thus, the only solution is $U(y) = 0$. We, therefore, require $k_c > p_{11} = \pi/2h_1$ for a guided wave solution. Now, k_c is in the range $\pi/2h_1 < k_c < \pi/2h_2$, so depending on h_2/h_1 it is possible to have more than one wave-like mode in the groove region where a particular k_c satisfies $p_{1,N} < k_c < p_{1,N+1}, N = 1,2,\cdots,M$, where $M = [k_c h_1/\pi + 1/2]$. Here, $[x]$ denotes the integer part of x. Thus, we can write $P_{1n} = -i\alpha_{1n} = -i(k_c^2 - p_{1n}^2)^{1/2}, n = 1,2,\cdots,M$ and (22) can be written as

$$\int_0^{h_2} U(t)K(y,t)\,dt = \sum_{n=1}^{M} V_n\psi_{1n}^{h,a}(y) \tag{24}$$

where for $m = 1,2,\cdots,M$

$$V_m = \frac{\chi(a, -i\alpha_{1m})}{i\alpha_{1m}h_1}\int_0^{h_2} U(y)\psi_{1m}^{h,a}(y)\,dy \tag{25}$$

and

$$K(y,t) = \sum_{n=M+1}^{\infty} \frac{\chi(a, P_{1n})}{P_{1n}h_1}\psi_{1n}^{h,a}(y)\psi_{1n}^{h,a}(t) + \sum_{n=1}^{\infty} \frac{1}{P_{2n}h_2}\psi_{2n}^{h,a}(y)\psi_{2n}^{h,a}(t). \tag{26}$$

Let us now define $u_n(y)$ to satisfy

$$\int_0^{h_2} u_n(t)K(y,t)\,dt = \psi_{1n}^{h,a}(y), \qquad n = 1,2,\cdots,M \tag{27}$$

where, from (24) and (25), we see that

$$V_m = \frac{\chi(a, -i\alpha_{1m})}{i\alpha_{1m}h_1}\sum_{n=1}^{M} V_n S_{mn}, \qquad m = 1,2,\cdots,M \tag{28}$$

where

$$S_{mn} = \int_0^{h_2} u_m(y)\psi_{1n}^{h,a}(y)\,dy, \qquad m,n = 1,2,\cdots,M. \tag{29}$$

It is convenient to write (28) in the matrix form

$$\boldsymbol{\Delta V} = \boldsymbol{SV} \tag{30}$$

where for $n = 1,\cdots,M$

$$\boldsymbol{\Delta} = \operatorname{diag}\left\{\frac{i\alpha_{1n}h_1}{\chi(a, -i\alpha_{1n})}\right\} \quad \boldsymbol{V} = \{V_n\}. \tag{31}$$

Then the condition corresponding to a guided wave is that (30) has a nontrivial solution or in the matrix form

$$\det(\boldsymbol{S} - \boldsymbol{\Delta}) = 0. \tag{32}$$

We now write (27) and (29) in an obvious operator notation

$$\mathcal{K}u_n = \psi_{1n}^{h,a}, \qquad n = 1,2,\cdots,M \tag{33}$$

and

$$(u_m, \psi_{1n}^{h,a}) = S_{mn}, \qquad m,n = 1,2,\cdots,M. \tag{34}$$

Now $S_{nm} = (u_n, \psi_{1m}^{h,a}) = (u_n, \mathcal{K}u_m) = (u_m, \mathcal{K}u_n) = S_{mn}$, since $K(y,t) = K(t,y)$, so $\boldsymbol{S} - \boldsymbol{\Delta}$ is a symmetric $M \times M$ matrix. Rather than solve (33) and (34) directly, we seek an

approximation $u_n \approx \tilde{u}_n$ such that $(\tilde{u}_m, \mathcal{K}\tilde{u}_n) = (\tilde{u}_m, \psi_{1n}^{h,a})$ where the approximation to S_{mn} is $\tilde{S}_{mn} = (\tilde{u}_m, \psi_{1n}^{h,a})$. Due to the positive definiteness of $\mathcal{K}$ it is possible to show that the approximation provides lower bounds on S_{mn}, i.e., $\tilde{S}_{mn} \leq S_{mn}$ as in, for example, [13] and [14].

The procedure for solution now follows. We know that k_c is in the range $\pi/2h_1 < k_c < \pi/2h_2$ with the possibility of M modes, which is dependent on h_1/h_2. Thus, for a fixed geometry we can determine the range of k_c and also the number of modes associated at a particular value of k_c. For example. we can show that $M = 1$ for $1 < h_1/h_2 \leq 3$ and thus, (32) reduces to solving

$$\boldsymbol{S} \equiv S_{11} = \boldsymbol{\Delta} = \frac{i\alpha_{11}h_1}{\chi(a, -i\alpha_{11})}. \tag{35}$$

Note from (13) that the right-hand side of (35) becomes $\alpha_{11}h_1 \tan \alpha_{11}a$ or $-\alpha_{11}h_1 \cot \alpha_{11}a$ corresponding to the symmetric and antisymmetric solutions about $x = 0$, respectively. Note that depending on a/h_1 or a/h_2 and because of the periodic nature of tan and cot we can have multiple solutions of k_c to (32) or (35).

We must first solve (27) or (33) and then determine S_{mn} from (29) or (34). We use an accurate Galerkin approximation which has proved successful in related problems [13], [14]. We begin by expanding u_m in a set of functions $b_r(y)$ such that

$$u_n(y) = \sum_{r=1}^{R} a_{nr} b_r(y), \qquad n = 1, 2, \cdots, M \tag{36}$$

and substitute in (27), multiply by $b_m(y)$ and integrate over $[0, h_2]$, to obtain for $n = 1, 2, \cdots, M, m = 1, 2, \cdots, R$

$$\sum_{r=1}^{R} a_{nr} K_{mr} = F_{mn}^{(1)} \tag{37}$$

where

$$K_{mn} = (\mathcal{K}b_n, b_m) = \sum_{r=M+1}^{\infty} \frac{\chi(a, P_{1r})}{P_{1r}h_1} F_{mr}^{(1)} F_{nr}^{(1)} + \sum_{r=1}^{\infty} \frac{1}{P_{2r}h_2} F_{mr}^{(2)} F_{nr}^{(2)} \tag{38}$$

and where for $i = 1, 2$

$$F_{mn}^{(i)} = (\psi_{\mathbf{in}}^{h,a}, b_m) = \int_0^{h_2} \psi_{\mathbf{in}}^{h,a}(y) b_m(y)\, dy \tag{39}$$

$$S_{mn} = \sum_{r=1}^{R} a_{mr} F_{rn}^{(1)}. \tag{40}$$

It remains to choose an appropriate form of the function $b_m(y)$. Now $b_m(y)$ is related to $u_m(y)$ by (36), which, in turn, originates from the decomposition of $U(y)$ in (20). It is easy to show from the singular behavior at the edge of the groove that $U(y) \sim Ay^{-1/3}$ as $y \to h_2$, thus, in order to correctly model the singularity at the edges of the guide we choose $b_m(y)$ as follows:

$$b_m(y) = \frac{(-1)^{(m+1)}(2m-1)!\Gamma(\frac{1}{6})C_{2m-1}^{1/6}(y/h_2)}{(2h_2)^{1/3}\pi\Gamma(2m-\frac{2}{3})(h_2^2 - y^2)^{1/3}} \tag{41}$$

where $C_m^{\nu}(y)$ are ultraspherical Gegenbauer polynomials satisfying

$$\int_0^1 \frac{C_{2m}^{\nu}(t)\cos zt}{(1-t^2)^{(1/2)-\nu}}\, dt = \pi \frac{\Gamma(2m+2\nu)J_{2m+\nu}(z)}{(-1)^m(2m)!\Gamma(\nu)(2z)^{\nu}} \tag{42}$$

$$\int_0^1 \frac{C_{2m+1}^{\nu}(t)\sin zt}{(1-t^2)^{(1/2)-\nu}}\, dt = \pi \frac{\Gamma(2m+2\nu+1)J_{2m+\nu+1}(z)}{(-1)^m(2m+1)!\Gamma(\nu)(2z)^{\nu}}. \tag{43}$$

See, for example, [16, p. 38]. Note that this choice of polynomial has a rather curious combination of factors in (41), but as we will see later [(44), (45)] is solely to achieve simplification of the final results.

It follows that

$$F_{mn}^{(i)} = (\psi_{\mathbf{in}}^{h,a}, b_m) = \frac{J_{2m-(5/6)}(p_{\mathbf{in}}h_2)}{(p_{\mathbf{in}}h_2)^{1/6}}, \qquad i = 1, 2. \tag{44}$$

Thus

$$K_{mn} = \sum_{r=M+1}^{\infty} \frac{\chi(a, P_{1r})}{P_{1r}h_1} \cdot \frac{J_{2m-(5/6)}(p_{1r}h_2)J_{2n-(5/6)}(p_{1r}h_2)}{(p_{1r}h_2)^{1/3}} + \sum_{r=1}^{\infty} \frac{1}{P_{2r}h_2} \frac{J_{2m-(5/6)}(p_{2r}h_2)J_{2n-(5/6)}(p_{2r}h_2)}{(p_{2r}h_2)^{1/3}}. \tag{45}$$

Note that it is not necessary to solve for the a_m. In an obvious matrix notation, we have from (37)

$$\boldsymbol{K}\boldsymbol{a}^T = \boldsymbol{F}^{(1)} \tag{46}$$

and

$$\boldsymbol{a}\boldsymbol{F}^{(1)} = \boldsymbol{S} \tag{47}$$

where

$$\boldsymbol{S} = \boldsymbol{a}\boldsymbol{K}\boldsymbol{a}^T = \boldsymbol{F}^{(1)^T}\boldsymbol{K}^{-T}\boldsymbol{F}^{(1)} = \boldsymbol{F}^{(1)^T}\boldsymbol{K}^{-1}\boldsymbol{F}^{(1)}. \tag{48}$$

Now, for a given geometry a, h_1, h_2 we find a range for k_c i.e., $\pi/2h_1 < k_c < \pi/2h_2$. We then seek solutions in this range from (32), where we note that the dimension (M) of $\boldsymbol{S}$ and $\boldsymbol{\Delta}$ changes depending on k_c. The matrix $\boldsymbol{\Delta}$ is given by (31), and $\boldsymbol{S}$ is calculated from (46)–(48) where $\boldsymbol{F}^{(i)}$ and $\boldsymbol{K}$ are given by (44) and (45). Note that we have to use R trial functions for the approximation and that the infinite sums for $\boldsymbol{K}$ have to be truncated. In Section III, we will show that we will only need about five trial functions and truncate the infinite sums to about 500 terms to achieve extremely accurate solutions with at least six decimal places of accuracy.

Now, for the TM modes, we follow a similar procedure by again matching ϕ_e and $\partial\phi_e/\partial x$, but this time we define $U(y) = (h_1h_2)^{-1}\phi_e(a, y)$ instead of the partial derivative of ϕ_e in the x-direction. The behavior of $U(y)$ at the edge of the groove changes from being singular to behaving like $U(y) \sim Ay^{2/3}$ as $y \to h_2$, so we choose $b_m(y)$ to reflect this. For the antisymmetric TM modes about $y = 0$ the main change is that

k_c is now in the range $\pi/h_1 < k_c < \pi/h_2$ with $M = [k_c h_1/\pi]$ and $Q_{1n} = -i\beta_{1n} = -i(k_c^2 - q_{\text{in}}^2)^{1/2}, n = 1, 2, \cdots, M$ and

$$\boldsymbol{\Delta} = \text{diag}\left\{\frac{\chi(a, -i\beta_{1n})}{i\beta_{1n}h_2}\right\}, \qquad n = 1, \cdots, M \tag{49}$$

$$F_{mn}^{(i)} = (\psi_{\text{in}}^{e,a}, b_m) = \frac{J_{2m+(1/6)}(q_{\text{in}}h_2)}{(q_{\text{in}}h_2)^{7/6}}, \qquad i = 1, 2 \tag{50}$$

where $b_m(y)$ is now chosen to be

$$b_m(y) = \frac{(-1)^{m+1}2^{2/3}}{\pi h_2^{7/3}} \frac{(2m-1)!\Gamma(\frac{7}{6})}{\Gamma(2m+4/3)}(h_2^2 - y^2)^{2/3} \cdot C_{2m-1}^{7/6}\left(\frac{y}{h_2}\right) \tag{51}$$

and

$$K_{mn} = \sum_{r=M+1}^{\infty} \frac{Q_{1r}h_2}{\chi(a, Q_{1r})} \cdot \frac{J_{2m+(1/6)}(q_{1r}h_2)J_{2n+(1/6)}(q_{1r}h_2)}{(q_{1r}h_2)^{7/3}} + \sum_{r=1}^{\infty} Q_{2r}h_1 \frac{J_{2m+(1/6)}(q_{2r}h_2)J_{2n+(1/6)}(q_{2r}h_2)}{(q_{2r}h_2)^{7/3}}. \tag{52}$$

For the TM modes symmetric about $y = 0$, k_c is now in the range $\pi/2h_1 < k_c < \pi/2h_2$ with $M = [k_c h_1/\pi + 1/2]$ and $P_{1n} = -i\alpha_{1n} = -i(k_c^2 - p_{\text{in}}^2)^{1/2}, n = 1, 2, \cdots, M$ and

$$\boldsymbol{\Delta} = \text{diag}\left\{\frac{\chi(a, -i\alpha_{1n})}{i\alpha_{1n}h_2}\right\}, \qquad n = 1, 2, \cdots, M \tag{53}$$

$$F_{mn}^{(i)} = (\psi_{\text{in}}^{e,s}, b_m) = \frac{J_{2m-(5/6)}(p_{\text{in}}h_2)}{(p_{\text{in}}h_2)^{7/6}}, \qquad i = 1, 2 \tag{54}$$

where

$$b_m(y) = \frac{(-1)^{m+1}2^{2/3}}{\pi h_2^{7/3}} \frac{(2m-2)!\Gamma(\frac{7}{6})}{\Gamma(2m+1/3)}(h_2^2 - y^2)^{2/3} \cdot C_{2m-2}^{7/6}\left(\frac{y}{h_2}\right) \tag{55}$$

and

$$K_{mn} = \sum_{r=M+1}^{\infty} \frac{P_{1r}h_2}{\chi(a, P_{1r})} \cdot \frac{J_{2m-(5/6)}(p_{1r}h_2)J_{2n-(5/6)}(p_{1r}h_2)}{(p_{1r}h_2)^{7/3}} + \sum_{r=1}^{\infty} P_{2r}h_1 \frac{J_{2m-(5/6)}(p_{2r}h_2)J_{2n-(5/6)}(p_{2r}h_2)}{(p_{2r}h_2)^{7/3}}. \tag{56}$$

III. Results

Before computing the results, the number of terms for the truncation of infinite series for K_{mn} and the number of trial functions R required to obtain accurate solutions are estimated. It was found that using the first 500 terms for K_{mn} for a given R gave results accurate to seven or eight decimal places. Using this truncation size, we found that just by using five trial functions ($R = 5$), solutions were obtained accurate to about seven decimal places. In Tables I and II, the ratio $\lambda_0/\lambda_z = \sqrt{1 - k_c^2/k_o^2}$ is calculated showing how rapidly the results converge for R for particular geometries. Also shown in the last rows of Tables I and II are the results obtained by Sachidananda [9] using a three-domain mode-matching technique showing that he was able to obtain two or three decimal places of accuracy (depending on how you round up or down). Although two or three decimal places are adequate for most plots, we will see later in Figs. 6–8 that a more accurate solution is required to differentiate between higher order modes, which at first glance appear to cross each other, but actually at closer inspection become very close (two decimal places) before separating.

TABLE I
Convergence of λ_0/λ_z with the Number of Trial Functions R for Varoius Geometries at a Frequency of 10 GHz. a) $h_2 = 0.2$ cm, $h_1/h_2 = 5, a/h_2 = 6$, b) $h_2 = 0.5$ cm, $h_1/h_2 = 2, a/h_2 = 2.4$, and c) $h_2 = 0.8$ cm, $h_1/h_2 = 1.25, a/h_2 = 1.5$. Also Shown are the Results by Sachidananda

R	a)	b)	c)
1	0.6532673	0.6142227	0.5903291
2	0.6532580	0.6142205	0.5901115
3	0.6532575	0.6142193	0.5901115
4	0.6532574	0.6142191	0.5901115
5	0.6532574	0.6142191	0.5901115
Sachidananda	0.65348	0.614928	0.590634

TABLE II
Convergence of λ_0/λ_z with the Number of Trial Functions R for Various Geometries at a Frequency of 20 GHz. $h_1/h_2 = 2$, a) $a = 0.2$ cm, $a/h_2 = 0.4$, b) $a = 0.5$ cm, $a/h_2 = 1$ and c) $a = 0.8$ cm, $a/h_2 = 1.6$. Also Shown are the Results by Sachidananda

R	a)	b)	c)
1	0.8784795	0.9060491	0.9142251
2	0.8782891	0.9060452	0.9142242
3	0.8782870	0.9060446	0.9142238
4	0.8782866	0.9060445	0.9142238
5	0.8782865	0.9060445	0.9142238
Sachidananda	0.878739	0.906235	0.914367

In Fig. 2, we have plotted $\lambda_c/4h_1 (= \pi/2k_c h_1)$ against h_2/h_1 when $a/h_1 = 0.4$ for the first TE mode (most dominant $M = 1$) symmetric about $x = 0$ along with the first-order theory of Nakahara and Kurauchi and Oliner's transverse equivalent network results. We see that Oliner's simple approximation is surprisingly accurate and that Nakahara and Kurauchi's results are not so good for large groove widths, but for smaller widths ($h_2/h_1 = 0.7$ to 1) their first-order theory is reasonably accurate. Also plotted in Fig. 2 are results for the small groove depth ($h_1/h_1 - 1 \ll 1$) approximation derived in the Appendix, and as we can see it is only accurate when $0.9 < h_2/h_1 < 1$. Note that in order to simplify the plot, only the most dominant mode is shown. In this case, the higher order modes would start appearing when $h_2/h_1 < 1/3$.

In Fig. 3, we have plotted λ_c against h_2 with $h_1 = h_2 + 10$ mm for the two cases (1) $a = 15$ mm and (2) $a = 5$ mm. Also plotted are the experimental results by Nakahara and Kurauchi and Oliner's equivalent network results. As we can see, our and Oliner's results agree very well with the experimental data.

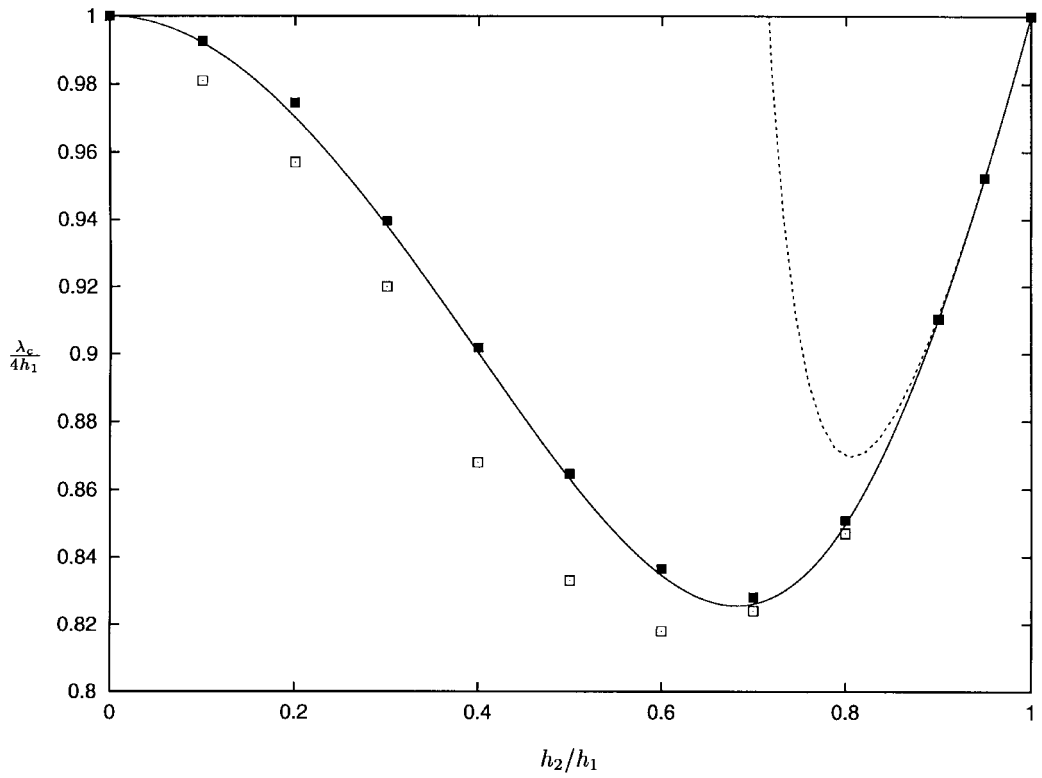

Fig. 2. The first TE solution symmetric about $x = 0$ with values of $\lambda_c/4h_1$ against h_2/h_1, — our results, - - - small $h_2/h_1 - 1$ approximation, ■ Oliner's equivalent circuit results, and □ for Nakahara and Kurauchi's results for $a/h_1 = 0.4$.

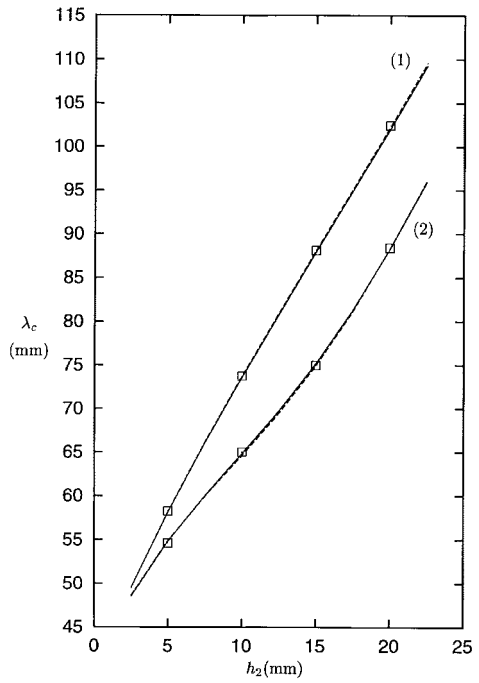

Fig. 3. Comparison between measured and theoretical values of λ_c against h_2, — our results, - - - Oliner's equivalent circuit results, and □ Nakahara and Kurauchi's experimental results with $h_1 = h_2 + 10$ mm for the two cases (1) $a = 15$ mm and (2) $a = 5$ mm.

In Fig. 4, we have plotted $k_c h_2$ against a/h_2 for the TE modes when $h_1/h_2 = 2$. Evans and Linton [17] considered an equivalent water wave problem and our results were originally compared with their Fig. 8, but after checking their results we found that they were computed incorrectly (private communication with Linton) and thus, no comparison could be made. Since $h_1/h_2 = 2$ the range of $k_c h_2$ is $[\pi/4, \pi/2]$ and we can only have one wave-like mode (in the x-direction, $M = 1$) in the groove region. Both symmetric and antisymmetric solutions about $x = 0$ are shown and as a/h_2 increases we see more and more modes exist. We can also see that the symmetric and antisymmetric modes alternate (and never cross) with the most dominant being the first symmetric mode. In fact, the first symmetric mode about $x = 0$ is the most dominant for all TE and TM solutions, as shown in Fig. 5. Here, results are plotted with $k_c h_2$ against a/h_2 for the symmetric about $x = 0$ solutions with $h_1/h_2 = 2$ (only one wave-like mode in x-direction) for the three types of modes: TE (most dominant), TM symmetric about $y = 0$, and TM antisymmetric about $y = 0$ (least dominant). It is obvious that the first symmetric about the $y = 0$ TM mode is least dominant since $\pi/h_1 < k_c < \pi/h_2$, but at first glance it is not so obvious whether the TE or the symmetric about $y = 0$ TM mode is most dominant since $k_c h_2$ lies in the range $\pi/2h_1 < k_c < \pi/2h_2$ for both modes. It is only by considering (35) and (49) where we seek solutions of $S_{11} = \alpha_{11} h_1 \tan \alpha_{11} a$ for the TE modes and $S_{11} = \cot \beta_{11} a / \beta_{11} a$ for the symmetric TM modes $(M = 1)$ that we find that the TE is in fact the most dominant ($k_c h_2$ is smallest) due to the behavior of $\cot$ and $\tan$.

So far, we have presented results with only one wave-like mode in the x-direction. When $h_1/h_2 > 3$ for the TE solutions,

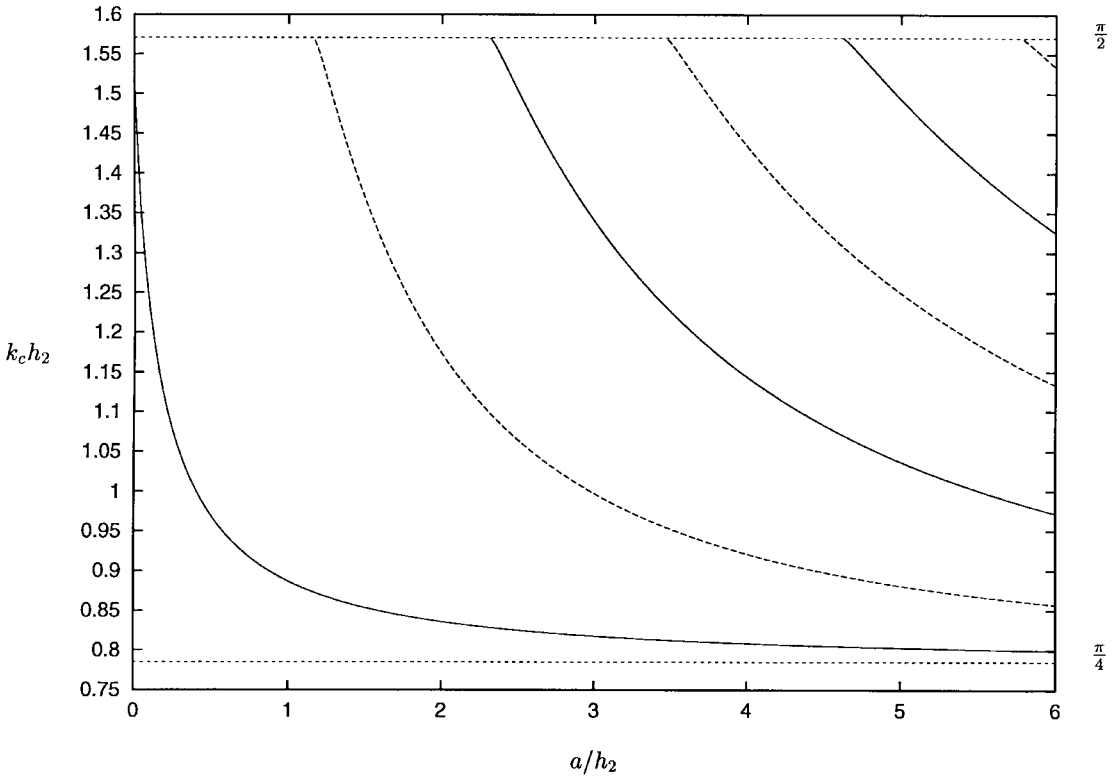

Fig. 4. TE solutions for values of $k_c h_2$ against a/h_2 with $h_1/h_2 = 2$, — symmetric, - - - antisymmetric about $x = 0$. Only one wave-like mode in groove region $(M = 1)$.

more wave-like modes in the x-direction appear $(M > 1)$, as shown in Fig. 6. Here, we have plotted $k_c h_2$ against a/h_2 where $h_1/h_2 = 6$ for the case of symmetry about $x = 0$. We first note that for any given a/h_2 there exist at least three values of the cutoff wavenumber $k_c h_2$. In fact, for all the TE modes there exist at least $M_{\max}$ solutions defined by

$$M_{\max} = \max_{\pi/2h_1 < k_c < \pi/2h_2} \left\{ \left[\frac{k_c h_1}{\pi} + \frac{1}{2} \right] \right\}$$

where $[x]$ denotes the integer part of x. As a/h_2 increases, more solutions appear as seen before in Figs. 4 and 5, but now with multiple wave-like modes in the x-direction the behavior of the cutoff wavenumbers has become more complicated. We also see that the curves plotted initially appear to cross each other at approximately $a/h_2 \sim 2.3$, 3, 4.2, and 5.2. A closer inspection reveals that the curves do not cross, but undergo a rapid change of direction ($k_c h_2$ decreases monotonically with increasing a/h_2) (A similar behavior occurs in a not entirely unrelated problem described by Dietz *et al.* [18]). For example, at the point where the curves nearly touch $a/h_2 \sim 4.21, k_c h_2 \sim 1.51$ the curves are within 0.1% (3/4 places of accuracy) of each other demonstrating the accuracy required in distinguishing between them.

For the TM modes, the behavior is slightly different. In Fig. 7, we have plotted $k_c h_2$ against a/h_2 with $h_1/h_2 = 3$ for the symmetric about $x = 0$, antisymmetric about $y = 0$ TM modes. For the case $h_1/h_2 = 3$ we can have two wave-like modes in the x-direction and as with the previous figure the curves of the cutoff wavenumbers become close at certain values of a/h_2. Here we find that we can have just one solution for the cutoff wavenumber for a given a/h_2 less than about 0.6. Here, the most dominant cutoff wavenumber can have either one or two wave-like modes in the x-direction, whereas the most dominant cutoff wavenumber for the TE solutions only has one wave-like mode in the x-direction. Note that by using just single-mode theory $(M = 1)$, one would conclude that no solution existed for a/h_2 less than about 0.85. Similar behavior is shown in Fig. 8 where we have plotted $k_c h_2$ against a/h_2 with $h_1/h_2 = 6$ for the symmetric about $x = 0$, antisymmetric about $y = 0$ TM solutions. Here we can have up to three wave-like modes in the x-direction and again the most dominant cutoff wavenumber can have either one, two, or three wave-like modes in the x-direction.

IV. Conclusion

In this paper, we have presented a full multimodal analysis of an open-ended rectangular groove waveguide for all forms of TE and TM modes. The problem was formulated in terms of an integral-equation representation to which a Galerkin approximation was applied using Gegenbauer polynomials as expansion functions which correctly model the field behavior at the sharp edges of the guide. The method of solution not only produced the most accurate results to date, but was also formulated in such a way that all cutoff wavenumbers including the higher order modes could be calculated.

Results were presented demonstrating the accuracy of the method and comparison with Nakahara and Kurauchi's exper-

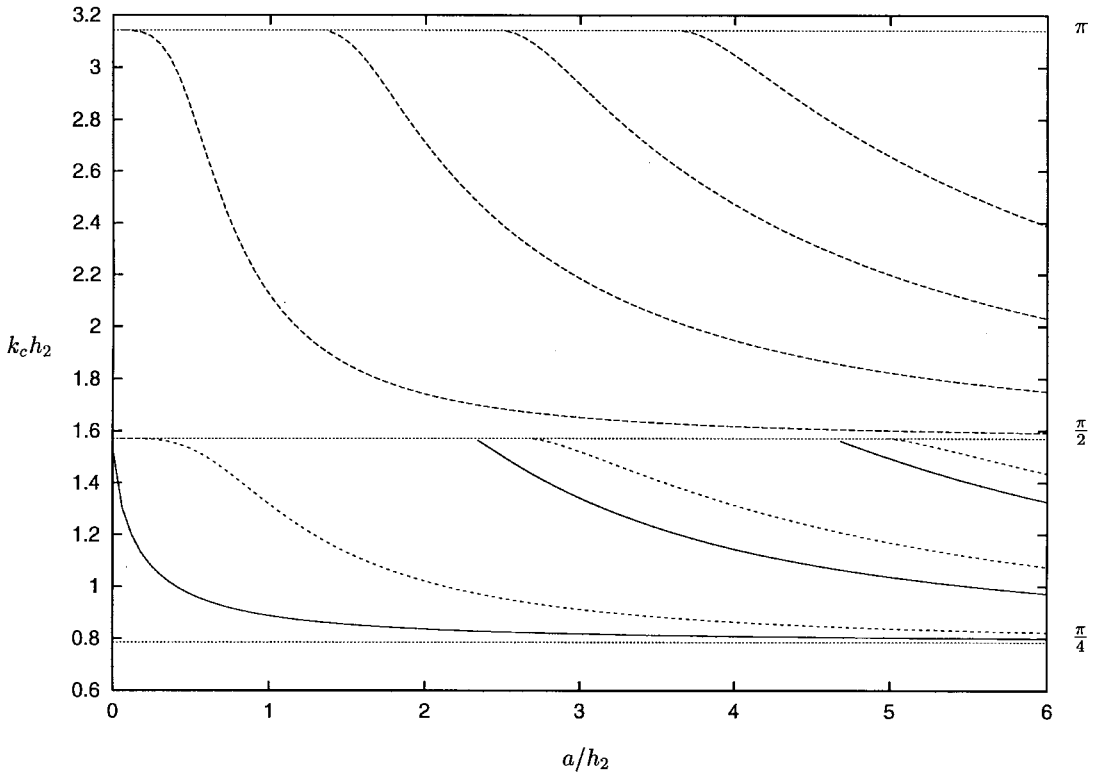

Fig. 5. Symmetric about $x = 0$ solutions for values of $k_c h_2$ against a/h_2 with $h_1/h_2 = 2$. — TE, - - - - - symmetric TM, - - - antisymmetric TM. For each case, only one wave-like mode in groove region.

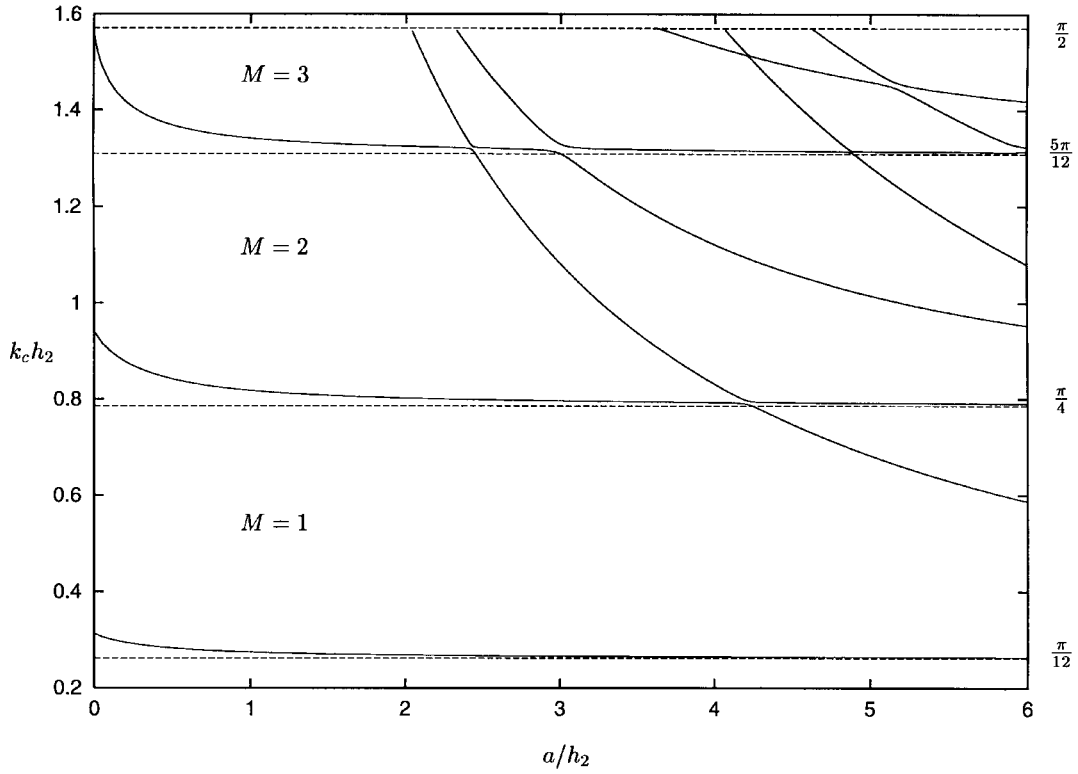

Fig. 6. Symmetric about $x = 0$ TE solutions for values of $k_c h_2$ against a/h_2 with $h_1/h_2 = 6$. Three wave-like modes in groove region $(M = 3)$.

imental data were made which show good agreement. Results have been presented for the multimodal solutions that show some remarkable behavior which might have been overlooked in a less accurate formulation. Finally, a simple small groove depth approximation has been developed which appears to give accurate results for $h_2/h_1 - 1 < 0.2$.

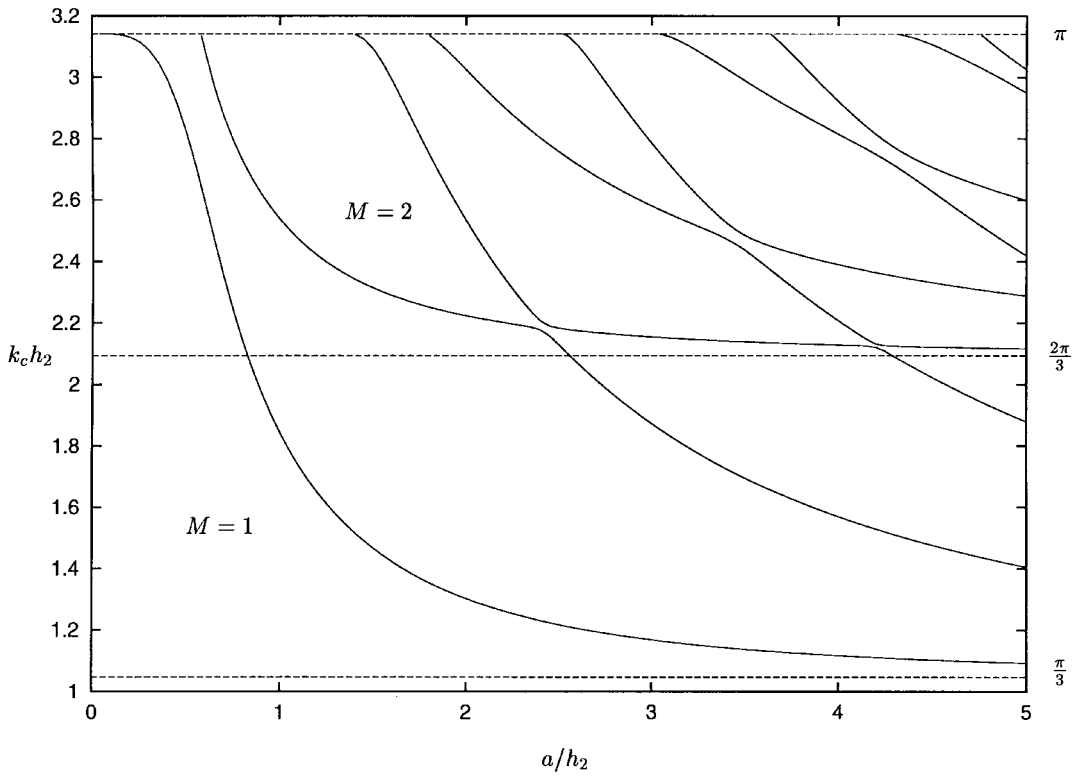

Fig. 7. Symmetric about $x = 0$, antisymmetric about $y = 0$ TM solutions for values of $k_c h_2$ against a/h_2 with $h_1/h_2 = 3$. Two wave-like modes in groove region ($M = 2$).

Appendix
Approximation for When the Groove Depth Is Small

Consider the arbitrary symmetric groove. We will consider the TE modes where we have the conditions $\phi_n = 0$ on the walls of the groove, $\phi = 0$ on the centerline $(y = 0), \phi \to 0$ as $|x| \to \infty$, and we look for solutions of the Helmholtz equation $(\nabla^2 + k_c^2)\phi = 0$. The shape of the wall is defined by $y = h_2 + \epsilon f(x)$ (ϵ small) where $f(-x) = f(x), f(x) \geq 0$ for $|x| \leq a$ and $f(x) = 0$ for $|x| > a$.

Now, taking the Fourier transform (FT) of the Helmholtz equation gives

$$\left(\frac{d^2}{dy^2} - \gamma^2\right)\Phi(\alpha, y) = 0, \qquad \gamma^2 = \alpha^2 - k_c^2 \tag{A.1}$$

where $\phi(x, y)$ is recovered from the inverse FT by

$$\phi(x, y) = \frac{1}{2\pi}\int_{-\infty}^{\infty} \Phi(\alpha, y) e^{-i\alpha x}\, d\alpha. \tag{A.2}$$

The solution of (A.1) satisfying the boundary condition $\Phi(\alpha, 0) = \phi(x, 0) = 0$ is given by

$$\Phi(\alpha, y) = \frac{1}{\gamma}\frac{\sinh \gamma y}{\cosh \gamma h_2}\int_{-a}^{a} \phi_y(t, h_2) e^{i\alpha t}\, dt \tag{A.3}$$

where we have used the FT of $\phi_y(x, y)$ at $y = h_2$. Now taking the inverse FT of (A.3), we obtain

$$\phi(x, y) = \int_{-a}^{a} \phi_y(t, h_2) M(x - t, y)\, dt \tag{A.4}$$

where

$$M(x, y) = \frac{1}{2\pi}\int_{-\infty}^{\infty} e^{-i\alpha x}\frac{\sinh \gamma y}{\gamma \cosh \gamma h_2}\, d\alpha = \sum_{n=1}^{\infty}(-1)^{n+1}\frac{e^{-\gamma_n x}}{\gamma_n h_2}\sin\left(n - \frac{1}{2}\right)\frac{\pi y}{h_2} \tag{A.5}$$

after we have integrated using residue calculus and where we have defined $\gamma_n = ((n - 1/2)^2\pi^2/h_2^2 - k_c^2)^{1/2}$. The remaining condition to be satisfied is $\phi_n = 0$ on $y = h_2 + \epsilon f(x)$ which can be written as

$$\phi_y(x, y) = \epsilon f'(x)\phi_x(x, y) \quad \text{on} \quad y = h_2 + \epsilon f(x). \tag{A.6}$$

Now expanding about $y = h_2$ using Taylor series we obtain

$$\phi_y(x, h_2) + \epsilon f(x)\phi_{yy}(x, h_2) = \epsilon f'(x)\phi_x(x, h_2) + \mathcal{O}(\epsilon^2) \tag{A.7}$$

and so ignoring terms of order ϵ^2 or greater, we obtain after substituting ϕ from (A.4)

$$\phi_y(x, h_2) = \epsilon\left\{f'(x)\int_{-a}^{a}\phi_y(t, h_2)M_x(x - t, h_2)\, dt - f(x)\int_{-a}^{a}\phi_y(t, h_2)M_{yy}(x - t, h_2)\, dt\right\}. \tag{A.8}$$

Let $\epsilon, \gamma_1 \to 0$ such that $\epsilon/\gamma_1 = \mathcal{O}(1)$. As $\gamma_1 \to 0$ the most dominant term in (A.5) can be shown to be $M_{yy}(x - t, h_2)$, namely

$$M_{yy}(x - t, h_2) \sim -\frac{1}{\gamma_1 h_2}\left(\frac{\pi}{2h_2}\right)^2 \tag{A.9}$$

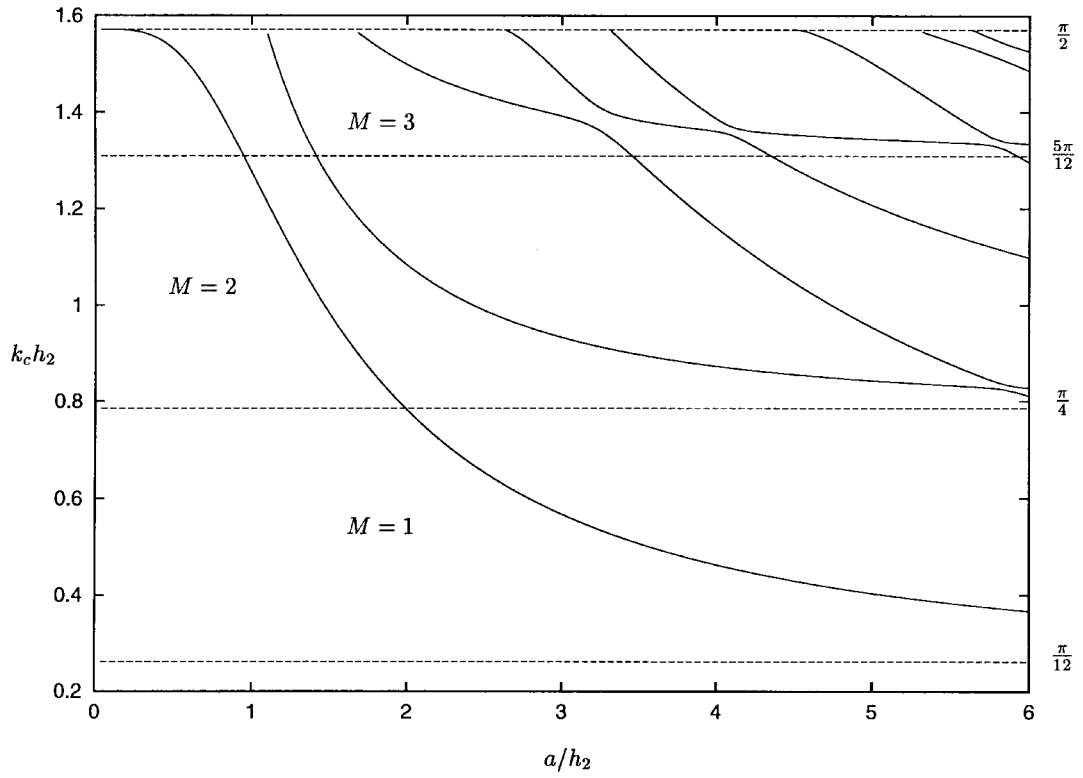

Fig. 8. Symmetric about $x = 0$, antisymmetric about $y = 0$ TM solutions for values of $k_c h_2$ against a/h_2 with $h_1/h_2 = 6$. Three wave-like modes in groove region $(M = 3)$.

and so as $\epsilon, \gamma_1 \to 0$

$$\phi_y(x, h_2) \sim \frac{\epsilon f(x)}{\gamma_1 h_2} \left(\frac{\pi}{2h_2}\right)^2 \int_{-a}^{a} \phi_y(t, h_2)\, dt. \tag{A.10}$$

Integrating with respect to x over $[-a, a]$ and canceling we find

$$\gamma_1 h_2 \sim \left(\frac{\pi}{2h_2}\right)^2 A \tag{A.11}$$

where A is the area of the groove region or

$$A = \epsilon \int_{-a}^{a} f(x)\, dx. \tag{A.12}$$

For the rectangular groove, $A = 2a(h_1 - h_2)$ and thus, (A.11) becomes for small $h_1/h_2 - 1$

$$k_c h_2 \sim \frac{\pi}{2} \sqrt{1 - \left\{\frac{\pi a}{h_2}\left(\frac{h_1}{h_2} - 1\right)\right\}^2}. \tag{A.13}$$

Following a similar procedure for the TM modes antisymmetric about $y = 0$ for the rectangular groove guide we find

$$k_c h_2 \sim \pi \sqrt{1 - \left\{\frac{2\pi a}{h_2}\left(\frac{h_1}{h_2} - 1\right)\right\}^2} \tag{A.14}$$

and for the TM modes symmetric about $y = 0$ we obtain the same approximation of the TE modes (A.13) for small $h_1/h_2 - 1$. These results agree with results contained in a recent paper of Bulla *et al*. [19] using functional analysis.

REFERENCES

[1] F. J. Tischer, "The groove guide, a low-loss waveguide for millimeter waves," *IEEE Trans. Microwave Theory Tech.*, vol. MTT-11, pp. 291–296, Sept. 1963.
[2] G. P. Bava and G. Perona, "Conformal mapping analysis of a type of groove guide," *Electron. Lett.*, vol. 2, no. 1, pp. 13–15, Jan. 1966.
[3] Y. M. Choi, D. J. Harris, and K. F. Tsang, "Theoretical and experimental characteristics of single V-groove guide for X-band and 100-GHz operation," *IEEE Trans. Microwave Theory Tech.*, vol. 36, pp. 715–723, Apr. 1988.
[4] T. Nakahara and N. Kurauchi, "Transmission modes in the grooved guide," *J. Inst. Elect. Commun. Eng. Japan*, vol. 47, no. 7, pp. 43–51, July 1964.
[5] ——, "Transmission modes in the grooved guide," *Sumitomo Electr. Tech. Rev.*, no. 5, pp. 65–71, Jan. 1965.
[6] A. A. Oliner and P. Lampariello, "The dominant mode properties of open groove guide: An improved solution," *IEEE Trans. Microwave Theory Tech.*, vol. MTT-33, pp. 755–764, Sept. 1985.
[7] S. F. Mahmoud, "Modal analysis of open groove guide," *IEEE Trans. Microwave Theory Tech.*, vol. 38, pp. 437–439, Apr. 1990.
[8] ——, *Electromagnetic Waveguides—Theory and Applications* (IEE Electromagnetic Waves Series 32). London, U.K.: Peregrinus, 1991.
[9] M. Sachidananda, "Rigorous analysis of a groove guide," *Proc. Inst. Elect. Eng.*, vol. 139, no. 5, pt. H, pp. 449–452, Oct. 1992.
[10] Z. Ma, E. Yamashita, and S. Xu, "Modal analysis of open groove guide with arbitrary groove profile," *IEEE Microwave Guided Wave Lett.*, vol. 2, pp. 364–366, Sept. 1992.
[11] Z. Ma and E. Yamashita, "A new method for the characterization of groove-guide leaky-wave antenna with an asymmetrically located metal strip," *IEEE Microwave Guided Wave Lett.*, vol. 2, pp. 489–491, Dec. 1992.
[12] ——, "Modal analysis of open groove guide with arbitrary groove profile," *IEEE Trans. Microwave Theory Tech.*, vol. 42, pp. 1925–1931, Oct. 1994.
[13] D. V. Evans and M. Fernyhough, "Edge waves along periodic coastlines. Part 2," *J. Fluid Mech.*, vol. 297, pp. 307–325, 1995.

[14] M. Fernyhough and D. V. Evans, "Scattering by a periodic array of rectangular blocks," *J. Fluid Mech.*, vol. 305, pp. 263–279, 1995.
[15] R. E. Collin, *Field Theory of Guided Waves*. New York: McGraw-Hill, 1960.
[16] A. Erdélyi, W. Magnus, F. Oberhettinger, and F. G. Tricomi, in *Tables of Integral Transforms*, vol. 1 (Bateman manuscript project). New York: McGraw-Hill, 1954.
[17] D. V. Evans and C. M. Linton, *J. Fluid Mech.*, vol. 225, pp. 153–175, 1991.
[18] B. Dietz, J. Eckmann, C. Pillet, U. Smilansky, and I. Ussishkin, "Inside-outside duality for planar billards—A numerical study," *Phys. Rev. E*, vol. 51, no. 5, pp. 4222–4231, 1995
[19] W. Bulla, F. Gesztesy, W. Renger, and B. Simon, "Weakly coupled bound states in quantum waveguides," to be published.

Mark Fernyhough was born in Worcester, U.K., in 1970. He received the B.Sc. degree in mathematics from the Royal College of Science, Imperial College, London, U.K., in 1991, and the Ph.D. degree in applied mathematics from the University of Bristol, Bristol, U.K., in 1994.

From 1994 to 1995, he worked at the University of Bristol as a Research Assistant. In 1996, he joined the Target Echo Strength Group, Defence Evaluation and Research Agency, Dorset, U.K. His research interests include trapped, edge, guided, and surface waves and scattering problems in the fields of linear water waves, acoustics, and electromagnetics.

David V. Evans was born in Hawarden, U.K., in 1940. He received the B.Sc. degree in mathematics and the Ph.D. degree in applied mathematics from Manchester University, Manchester, U.K., in 1962 and 1966, respectively.

In 1964, he was appointed an Assistant Lecturer of mathematics at Manchester University. In 1967, he moved to the United States, spending a year at the Davidson Laboratory, Stevens Institute of Technology, Hoboken, NJ, before moving to the Department of Naval Architecture (now Ocean Engineering) at the Massachusetts Institute of Technology (MIT), Cambridge, where he worked from 1968 to 1969. Since 1969, he has worked in the Department of Mathematics, University of Bristol, Bristol, U.K., first as a Lecturer, then as a Reader in 1979, and since 1986, as a full Professor. His research interests are in the field of linear water waves, acoustics, and boundary-value problems.